Electrical Properties of Carbon Fiber Support Systems

W. Cooper [a] M. Demarteau [a,*] K. Hanagaki [a] M. Johnson [a,*]
M. Matulik [a] A. Nomerotski [a] B. Quinn [b]

[a] *Fermi National Accelerator Laboratory, Batavia, IL 60510*

[b] *University of Mississippi, University, MS 38677*

Abstract

Carbon fiber support structures have become common elements of detector designs for high energy physics experiments. Carbon fiber has many mechanical advantages but it is also characterized by high conductivity, particularly at high frequency, with associated design issues. This paper discusses the elements required for sound electrical performance of silicon detectors employing carbon fiber support elements. Tests on carbon fiber structures are presented indicating that carbon fiber must be regarded as a conductor for the frequency region of 10 to 100 MHz. The general principles of grounding configurations involving carbon fiber structures will be discussed. To illustrate the design requirements, measurements performed with a silicon detector on a carbon fiber support structure at small radius are presented. A grounding scheme employing copper-kapton mesh circuits is described and shown to provide adequate and robust detector performance.

Key words: carbon fiber, silicon vertex detector, support structure, grounding, Tevatron, Fermilab, Dzero
PACS: 29.40.Gx, 29.40.Wk, 29.90.+r, 72.80.Tm, 81.05.Uw

1 Introduction

Nowadays carbon fiber is a ubiquitous structural material used in a wide range of applications due to its high modulus and low mass. It offers great flexibility in terms of tuning thermal and mechanical properties through the orientation

* Tel.: 630-840-2840 (Demarteau), 630-840-3168 (Johnson)
Email addresses: demarteau@fnal.gov (M. Demarteau), mjohnson@fnal.gov (M. Johnson).

and number of lay-ups of the fibers. Carbon fiber support structures have also become common elements of detector designs for high energy physics experiments and are especially prevalent in the design of silicon vertex detectors. Early examples of the use of carbon fiber in external support structures are the DELPHI silicon detector [1], the space frames for the BaBar [2] and CDF ISL silicon detector [3]. In current designs, carbon fiber is integrated in the design of silicon detector modules, like the readout modules for the silicon tracker for the CMS experiment [4]. An example of a detector with a fully integrated carbon fiber support structure is the Layer 00 detector for the CDF collaboration at the Fermilab Tevatron collider [5].

While the use of carbon fiber solves a variety of mechanical problems, it presents a challenging set of electrical concerns. Highly conductive carbon fiber surfaces produce an undesirable capacitance relative to sensors, electronics and cables and can compromise the detector performance due to significant coherent noise pickup [6]. Well-designed coupling and grounding schemes are essential for producing low-noise environments for these detectors.

Here we describe the electrical characteristics of carbon fiber as applicable to a silicon tracker at small radius with an integrated carbon fiber support structure. Measurements are performed on a prototype of a detector that has been proposed for the DØ experiment at the Fermilab Tevatron collider, called the Layer Zero (LØ) detector [7].

2 Detector Design

The design of the LØ detector calls for the silicon sensors to be mounted directly on a full length carbon fiber support structure at a radius of about 17 mm. Sensors with p-implants on an n-type substrate with 50 μm readout pitch, 8 cm long, produced by ELMA [8], were used in the study. The sensors have 256 readout strips. A low-pass filter card of 150 μm thick G-10 for the bias high voltage and bias return is glued directly onto the sensor, close to the wire bonding pads.

Often the hybrid with the front-end readout electronics is mounted directly on the sensor. In this design, due to space constraints and heat dissipation, the signals from the silicon sensors are transmitted to the hybrid containing the readout chips by flexible circuits up to 435 mm long. Since these circuits carry analogue signals they are referred to as 'analogue cables'. Although this solution is very attractive because of reduced material and heat generation in the sensitive volume, it represents a considerable technical challenge. The addition of the analogue cable reduces the signal to noise of the silicon sensors due to the added capacitive load. Procurement of the flex cables and the

complicated ladder assembly are other non-trivial issues.

One of the most important aspects in the design and technical realization of a long analogue cable is the capacitance between the traces, which should be as small as possible to optimize the S/N ratio. Our design uses a stack of two cables with constant 91 μm pitch, laminated with a lateral shift of 45 μm. The pitch of the cable stack thus matches the pitch of both the readout strips on the sensor and of the input bond pads on the front-end readout chip. It should be noted that with this configuration adjacent readout channels alternate between the top and bottom cable in the stack. Stated in an different way, all odd readout channels are connected to one cable in the stack and all even channels to the other cable. For our configuration, the first channel is channel 1, and all odd channels (1, 3, 5, ...) correspond to the top cable in the stack. In order to reduce the capacitance contribution from the adjacent cable within the stack of two cables, a spacer consisting of 150 μm thick polypropylene mesh with about 25% volume occupancy is placed between the two cables. After a series of prototypes, flawless cables were produced by Dyconex [9]. The capacitance as measured for this arrangement is 0.36 pF/cm in good agreement with ANSYS [10] calculations. In our setup we used 42 cm long prototype cables. Each cable has 129 signal traces with 91 μm pitch. Each trace is 16 μm wide copper on a 50 μm thick kapton substrate. One trace is reserved as a spare trace in case of an open. Two additional, wider traces (100 μm) are provided on the cable for the bias voltage and its return.

The analogue cable is wirebonded to a ceramic hybrid containing two SVX4 readout chips with 128 input channels each. The SVX4 chip is the fourth generation front-end readout chip for silicon strip detectors developed for the extended run at the Fermilab Tevatron [11]. The chip operates at 53 MHz, amplifies the signals and stores them on a 48 cell deep pipeline for readout. A Wilkinson-type ADC digitizes the signals and I/O circuitry allows for sparsified readout. The equivalent noise charge (ENC) of the SVX4 chip is $300 + 41 * C(\mathrm{pF})$ (e^-), at a fixed risetime of 69 ns. The digital signals from the hybrid are transmitted to a flexible cable through a 50-pin 2.5 mm high AVX connector [12] to the data acquisition system.

In the next section the electrical characteristics of carbon fiber will be described. The carbon fiber test pieces were made using carbon fiber epoxy resin prepregs using K139, obtained from Bryte [13], and K13C, obtained from YLA [14]. The carbon fiber in both products was manufactured by Mitsubishi. K139 uses 110 Msi modulus fiber with a thermal conductivity of 210 W/mK, with a fiber aerial weight (FAW) of 55 g/m^2. K13C has a modulus of 130 Msi, with a significantly higher thermal conductivity of 620 W/mK and a FAW of 69 g/m^2 [15]. For both prepregs, the resin fraction is about 35% by weight, or roughly 50% by volume before curing.

Based on the results of the electrical tests of the carbon fiber, methods will be outlined that address the electrical requirements for the construction of support structures for silicon detectors. The design addresses all potential noise sources. Tests aimed at minimizing coherent noise contributions with a full-scale silicon detector, populated with a limited number of readout modules will be described. The paper concludes with a suggested set of design rules which need to be respected in the construction of silicon detectors with integrated carbon fiber supports.

3 Electrical Conductivity of Carbon Fiber

Carbon fiber with ultra-high modulus ($\sim$1000 GPa) also has low resistivity (100 Ωcm) [15]. These materials are characterized by particularly high conductivity at high frequency with associated design issues. A series of tests were carried out to verify the conductivity of carbon fiber.

The first study performed was a measurement of capacitor impedance. Two parallel plate capacitors were built using $6'' \times 6''$ bare FR4 cores, with $\epsilon_r = 4$, approximately $0.27''$ thick. The first capacitor, used for baseline measurements, had two tinned copper electrodes laminated to either side of the FR4 dielectric. Each electrode is approximately $0.075''$ thick. The second capacitor has a single tinned copper electrode attached to one side of the FR4 dielectric and a single carbon fiber electrode attached to the other side. The carbon fiber electrode was four plies of K139 fiber with a 4-layer $[0^0/90^0]_s$ lay-up, approximately $0.04''$ thick. Contact with the two electrodes of the capacitor under measurement was established using two 20AWG stranded wires connected to the two contacts of a BNC connector. For the capacitor electrode side, the strands were separated and splayed to maximize contact and taped to the electrode with a specific area of copper tape. Prior to the attachment of the probe, the contact area on the electrode was burnished with mildly abrasive polishing material (Scotch-Brite) and cleaned with isopropyl alcohol. After taping the probe to the electrode, the tape was worked with a blunt tool to maximize contact to the strands of the probe and to force air from under the copper tape to the outside edge to maximize contact to the electrode. Past experience has shown that not taking care at this stage in the test preparation would result in inconsistent measurements. The size of the copper tape used to make contact with the carbon fiber electrode was varied to measure the effect of the fraction of contact area required to obtain a given impedance response.

Impedance measurements were then made using an HP4193A Vector Impedance meter at specific frequencies over a range of 0.4 to 110 MHz. The measurements were performed in a temperature and humidity controlled environment. The measured impedance and phase shift is shown in Fig. 1 for six different capac-

itors: the reference capacitor with two copper electrodes, and the capacitors with one copper electrode and one carbon fiber electrode with a copper tape contact area of 1, 2, 4, 9 and 36 square inches. The inset shows a blow-up of the region around the minimum. For low frequencies, the behavior is the expected $1/j\omega C$ dependence. In this frequency range, from 0.4 to 50 MHz, the response of all capacitor configurations is virtually identical. With increasing frequency the impedance decreases rapidly and reaches a minimum with vanishing phase shift. At this point the impedance is real and purely resistive. The reference capacitor with two copper electrodes reaches the lowest impedance of all configurations. The capacitor configurations with one carbon fiber electrode with a copper area of 4, 9 and 36 in^2 are virtually indistinguishable.

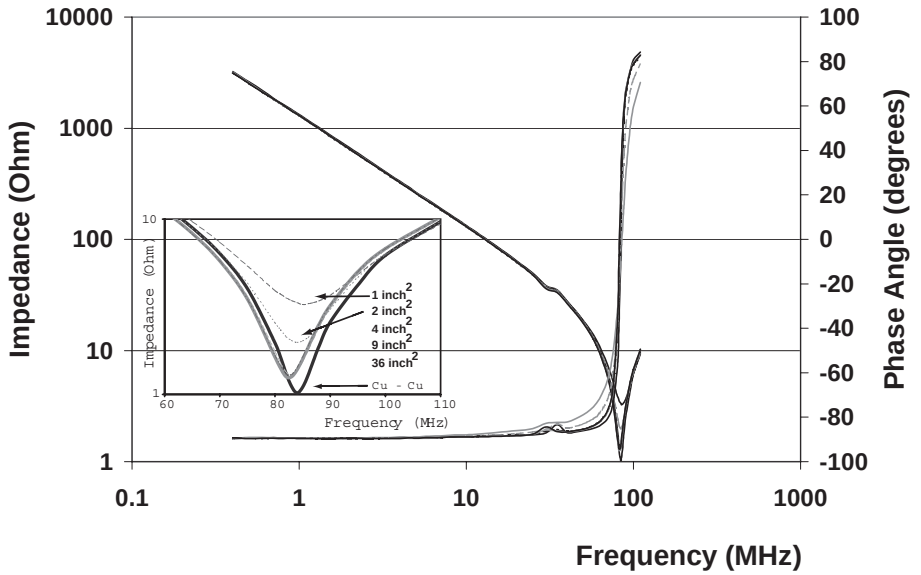

Fig. 1. Impedance and phase shift as function of frequency for different configurations of parallel plate capacitors.

Plotting the value of the minimum of the impedance from Fig. 1 as function of fractional copper contact area of the carbon fiber gives the result shown in Fig. 2. The frequency at which the impedance minimum occurred was at 84±1 MHz for all capacitor configurations tested. The impedance of the reference capacitor, with dual copper electrodes, is 1.02 Ω and is indicated by the solid line. The results show that at high frequencies, the frequencies of interest for silicon vertex detectors, carbon fiber is to be regarded as a conductor. Furthermore, a 15-20% area coverage of the carbon fiber with a good conductor should provide adequate electrical coupling to the carbon fiber.

The measurements were also performed by placing the capacitors in a bandstop circuit and measuring the power transfer function with an HP3577A network analyzer as function of frequency. The results are in complete agreement with the results quoted above.

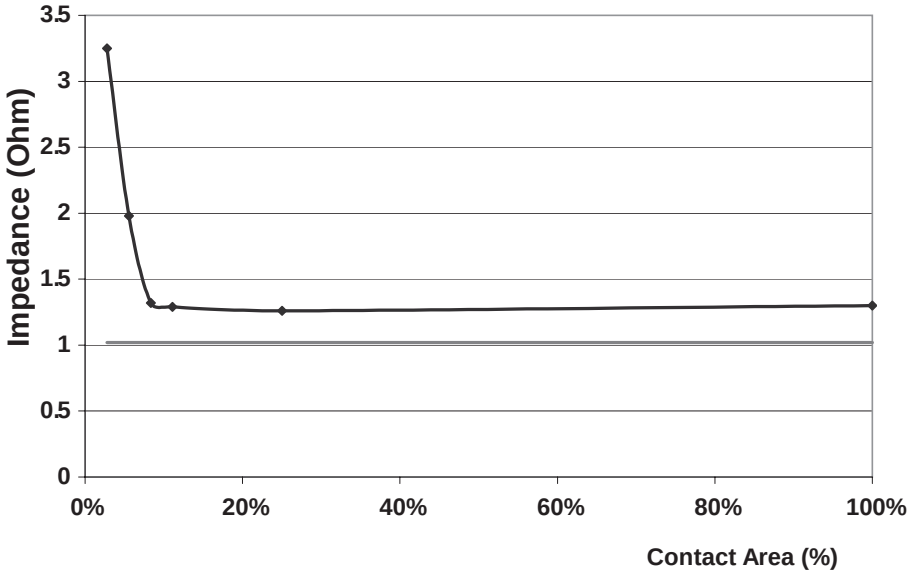

Fig. 2. Impedance of parallel plate capacitors as function of the copper area on the second, carbon fiber, electrode (see text for details).

To verify that the carbon fiber was not acting as part of the dielectric, another measurement was taken with the carbon fiber completely removed and with the 1 by 2 inches copper tape directly attached to the FR4 sheet. The frequency response of the impedance for this configuration, together with the response of the reference capacitor with two copper electrodes, is shown in the upper half of Fig. 3. The upper impedance curve corresponds to the capacitor with the carbon fiber removed and replaced with copper tape with an area of 2 in^2. The difference between the measured impedance for the two configurations, compared to the frequency response with the carbon fiber sheet (see Fig. 1) is striking and clearly shows that the carbon fiber does not act as part of the dielectric. The lower half of Fig. 3 shows the capacitance for the two configurations as function of frequency, corrected for the contribution from the test setup. Given an area ratio of 18 for the two configurations (36 in^2 versus 2 in^2) the ratio of the two capacitance values is naively expected to be a factor of 18. A ratio of 11.9 is measured, however. The electrical field configuration for the capacitor with a 2 in^2 copper area taped to a 36 in^2 dielectric with a 36 in^2 opposite copper electrode is expected to be very different from a uniform parallel plate capacitor with two 36 in^2 copper electrodes.

To understand the measurement, a full ANSYS calculation was performed. Using ANSYS, the capacitance of the 6 by 6 inch capacitor with the copper electrodes was calculated to solve for the dielectric constant of FR4. Based on the measured value of 117 ± 6 pF, the ANSYS calculation gives a value for the dielectric constant of 3.6 ± 0.2. Using the simple analytic formula for the capacitance of area over separation, a value of 3.9 is obtained. Using the value of 3.6 for the dielectric constant, ANSYS predicts a capacitance of 8.0 pF for the capacitor with the 2 in^2 copper electrode, whereas the measured value,

corrected for capacitance of the leads, is 9.8 ± 1.5 pF. The contributions to the error estimate are a 10% error on the measurement itself, a 10% error on the correction due to the test fixture, and a 5% error on the extraction of the dielectric constant, added in quadrature. The measured ratio of capacitances of 11.9 ± 1.9 is in reasonable agreement with the predicted ratio of 14.6, validating our conclusion that carbon fiber does not act as part of the dielectric.

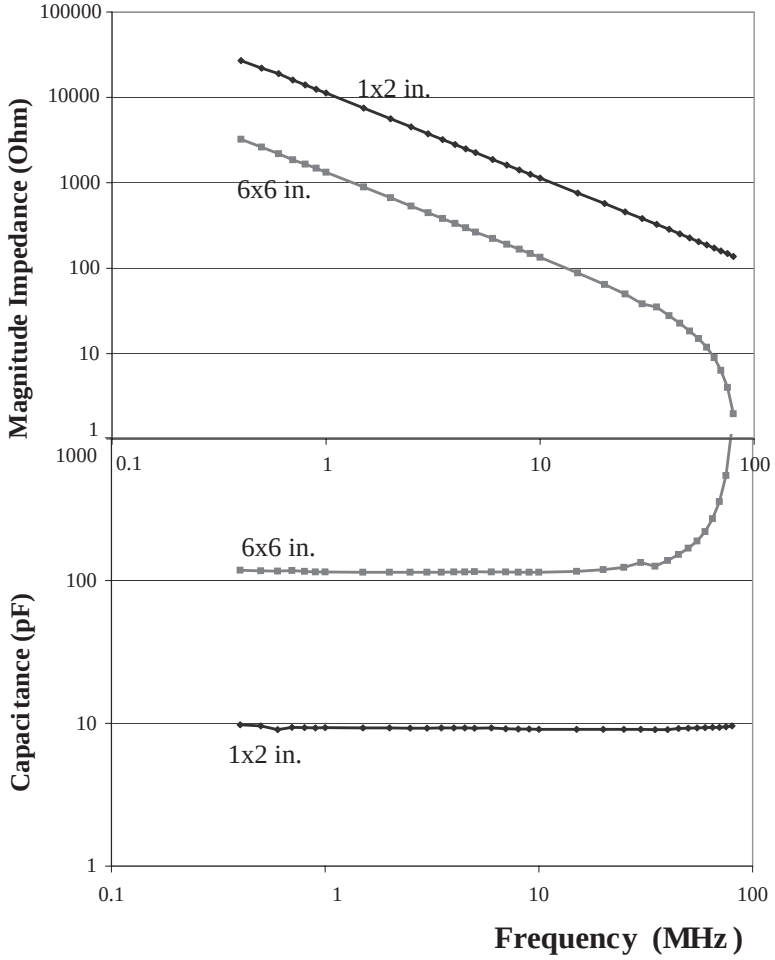

Fig. 3. Impedance and capacitance as function of frequency for two different configurations of parallel plate capacitors. The top (bottom) curve in the upper (lower) plot corresponds to the capacitor with the carbon fiber plate removed and replaced with a 2 in^2 piece of copper directly attached to the dielectric; the other curves correspond to the capacitor with two copper electrodes.

It is to be concluded from these studies that carbon fiber should be regarded as a conductor for the frequency range of interest for our application of 5 kHz to 50 MHz. Using highly conductive carbon fiber as a mechanical support thus has the potential to exhibit strong capacitive coupling to the silicon sensors it supports, which can lead to very troublesome sources of noise, especially in close-packed structures. It is therefore imperative that all the carbon fiber in

the detector is effectively shorted to the hybrid or bias filter grounds to prevent noise transmission through capacitive coupling to the sensor readout. It has been demonstrated that copper in contact with the carbon fiber with more than 10-15% area coverage provides adequate electrical coupling. In the next section methods to apply our findings to the construction of silicon detector modules will be explored.

4 Development of Grounding Method

In the design of the silicon detector, the ground plane of the sensor, and the carbon fiber support structure form the plates of a parallel plate capacitor. This puts the sensors between two plates of a capacitor, and any power transfer through the capacitor caused by unequal potential at its plates will generate noise on the sensor. The challenge is to devise a low mass short between the carbon fiber and ground plane which is highly efficient over a frequency range of 5 kHz - 50 MHz. To determine the feasibility of shorting the carbon fiber support cylinder, on which the silicon sensors are mounted, to the hybrid or filter ground plane, a series of tests were carried out with a mockup of the real design.

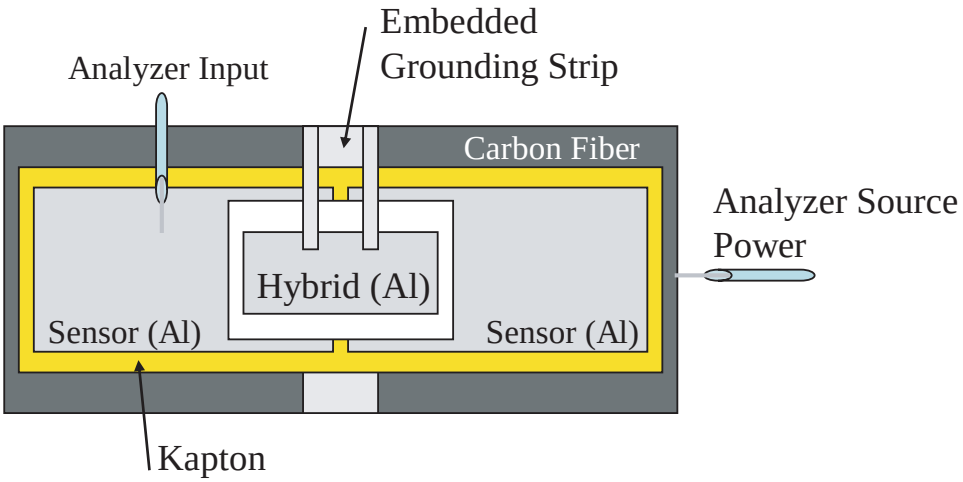

Fig. 4. Sketch of the mockup of the detector for the coupling study. Silicon sensors and the ground plane on a bias voltage filter card or hybrid are modeled using 0.5 mil thick aluminum strips, separated by a non-conducting plastic. This sketch shows the configuration of one aluminum strip on the carbon fiber support. Up to four strips of three different materials were used.

A mock-up of the carbon fiber support/sensor/ground plane configuration was built (see Fig. 4). Two pieces of 0.5 mil aluminum (indicated by 'Sensor (Al)' in Fig. 4) representing two sensors, were attached to a strip of kapton, that was mounted directly onto a carbon fiber support structure. This carbon fiber support piece has a 6-layer $[0^0/+20^0/-20^0]_s$ lay-up of K13C high modulus

carbon fiber. It should be noted that K13C is even more conductive than K139. A piece of plastic, mimicking the filter card or hybrid, was laid on top of the 'sensors'. A thin 0.5 mil aluminum foil was attached to the plastic representing the ground plane (indicated by 'Hybrid (Al)' in Fig. 4). The carbon fiber support was driven with the source power from the network analyzer. The network analyzer input was wired to the sensor aluminum layer and both the source and input grounds were connected to the filter plane ('Hybrid (Al)' in Fig. 4). Power transfer functions were measured with different configurations for shorting the carbon fiber to the filter plane. One to four $\frac{1}{8}''$ wide strips of 1 mil thick aluminized Mylar, 0.5 mil aluminum, or 1 mil copper grounding strips were attached between the kapton and the carbon fiber. The aluminized Mylar had a 250-300 Å thick layer of pure aluminum. Short strips of the same material were attached to the grounding strips. In the study, these strips were then wrapped around the 'sensors' and attached to the filter/hybrid ground plane (see Fig. 4).

First, a reference power transfer function was measured with no grounding strips attached. Next, the grounding strips were attached one by one, varying area of the carbon fiber covered with grounding strips, and the power transfer was measured again. It was found that aluminized Mylar strips were minimally effective in reducing power to the sensor. Aluminum and copper strips performed equally well. The power reduction was independent of the number and size of strips, but proportional to the area used to couple the strips to the carbon fiber. We achieved a maximum reduction in excess of 40 dB at 1 MHz with copper tape covering about 11% of the carbon fiber, identical to the result shown in the previous section (see Fig. 2).

Because copper tape coupling would not be feasible in the detector due to mass constraints, the next coupling test was carried out using carbon fiber pieces with embedded aluminum foil and aluminized Mylar. The aluminum or Mylar was attached to the carbon fiber by co-curing it with the carbon fiber. A new sensor/hybrid mockup was built and mounted on different pieces of K13C carbon fiber which had various amounts of surface area covered with embedded aluminum or aluminized Mylar. The embedded grounding material, as before, extends out to grounding strips that fold over and attach to the hybrid/filter plane, as sketched in Fig. 4. It was noticed that aluminized Mylar grounding produced significantly less attenuation than aluminum; about 10 dB less below 20 MHz. This test also verified that the attenuation is not affected by the width of the grounding strips. Measurements of transfer functions were taken with different areas of embedded aluminum and equal sized grounding strips. Those data confirmed that the attenuation increases with contact area to the carbon fiber. The maximum area of embedded aluminum tested was about 4 in^2 (again, about 11% of the area), giving a power decrease of at least 30 dB for all frequencies below 50 MHz.

Although coupling to carbon fiber through embedded aluminum has thus been shown to be an effective grounding technique, the use of aluminum does not represent a robust solution. The aluminum is very susceptible to oxidation and the likely choice for contacts to the ground plane would be silver epoxy, which historically has not been particularly reliable. This has led us to the design which employs a kapton flex circuit with a copper mesh, embedded in the carbon fiber surface. To obtain a more robust design we opted for a configuration where the kapton covers the surface area completely, with the embedded copper mesh having only a limited area coverage.

5 Full Prototype Experimental Setup

A full-size prototype crenellated two-part support structure was made using K13C fiber. It consists of a twelve-sided inner shell and a six-sided outer shell. The inner shell has a 4-layer $[0^0/90^0]_s$ lay-up of K13C high modulus carbon fiber. The outer shell has a 6-layer $[0^0/+20^0/-20^0]_s$ lay-up of the same high modulus fiber. The inner shell extends beyond the length of the outer shell and forms the support structure for the hybrids. The outer shell only supports the sensors (see Fig. 7). A 0.025 mm kapton sheet with an embedded copper mesh was co-bonded to the outer shell for grounding connections. The copper mesh, 5 μm thick, which is in direct contact with the carbon fiber, has an area coverage of 30%. Round copper pads, one for each sensor, are provided on the top side of the mesh. The pads are nickel-gold plated, with a thickness of 1.3 μm and 0.3 μm, respectively. Four vias, with 0.889 mm diameter holes establish the electrical connection between the pad and the copper mesh. Four vias were chosen to lower the inductance and for redundancy. The top drawing in Fig. 5 shows one end of the copper-mesh cable, produced by Compunetics [16].

An insulating two-layer kapton flex circuit, shown in the lower drawing in Fig. 5, is glued to the backside of the sensors, covering the backside completely. This circuit, also produced by Compunetics, has one tab on either side that wraps around the sensor and is attached to the filter card mounted on the sensor. The right angles in the drawing indicate where the kapton is trimmed, so that the full backside of the sensor is covered by kapton. After the backside lamination, the sensor is mounted on the support structure with the embedded mesh. The tab connected to the round pad in the bottom drawing in Fig. 5 picks up the bias voltage from the filter card and directly applies it to the backside of the sensor. The small rectangular pad connected to the larger rectangular pad is the ground connection. The smaller rectangular pad has three 0.889 mm vias which establish the connection to the co-bonded copper mesh of the outer shell of the support structure. Figure 6 show a schematic cross section of a sensor mounted on the support structure to aid in the understanding how all electrical connections are established.

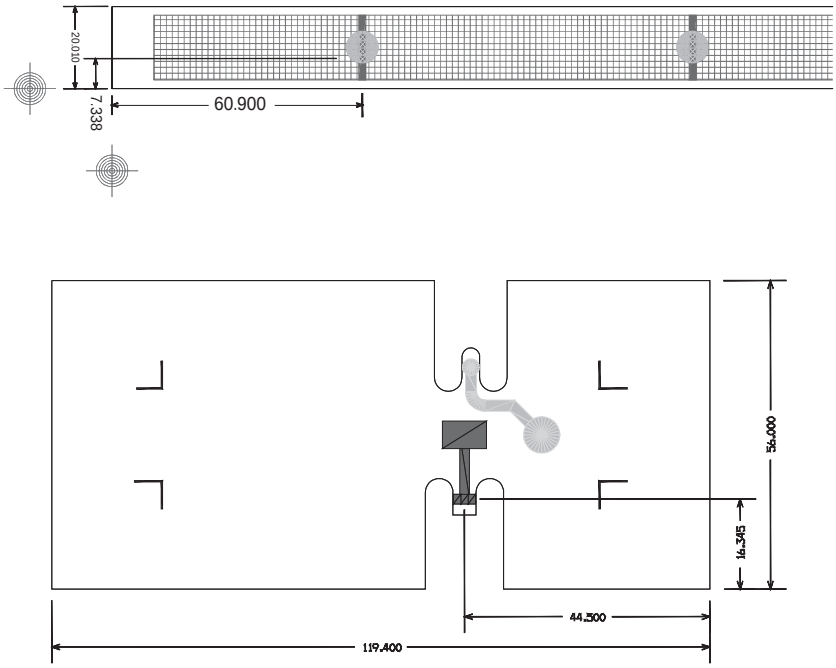

Fig. 5. Drawing of the copper mesh cable that was embedded in the carbon fiber support structure (top); drawing of the sensor 'wrap-around' flex circuit (bottom).

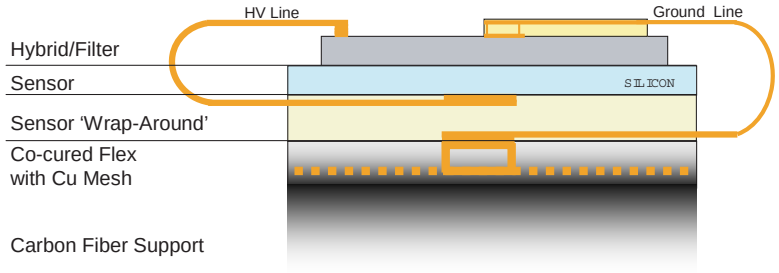

Fig. 6. Schematic cross section of the electrical configuration (drawing not to scale).

The twelve-sided inner shell of the support structure is longer than the crenellated outer shell and forms the support structure for the hybrids. A separate kapton-copper mesh, with the same specifications as the circuit for the sensor support, was embedded in the carbon fiber to provide the ground for the hybrids. At the transition between the sensor and hybrid support regions the two copper mesh circuits can be connected electrically through a small jumper mesh cable. It should be noted that in our initial tests, described below, the two ground mesh circuits were not connected. Fig. 7 shows a detail of the solid model of the transition region between sensor and hybrid support regions.

The silicon sensors are mounted on the outer shell with the embedded grounding copper-kapton mesh using epoxy. The p-side of the sensor was grounded

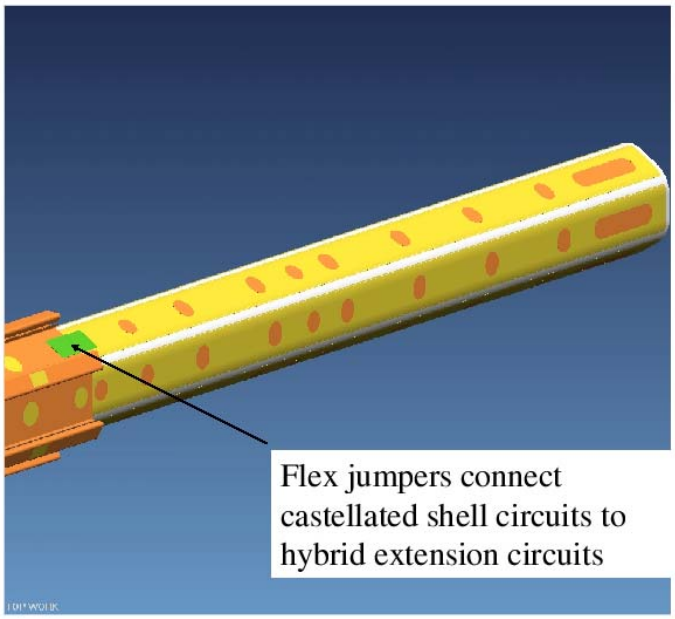

Fig. 7. Solid model of the transition region between sensor and hybrid support. The separate embedded ground mesh circuits are visible. Also indicated is the jumper cable to electrically connect the two separate ground mesh circuits.

to the carbon fiber support structure through the embedded copper-clad kapton flex circuit as described above: the rectangular ground tab on the 'wrap-around' flex circuit was attached to the biasing filter card, that was glued on top of the sensor, and the round pad on the backside sensor lamination picks up the sensor bias voltage (see Fig. 6). The sensor bias line was wirebonded to the ground pad on the bias filter card. The two-layer analogue cable was wirebonded to the sensor at one end and to the ceramic hybrid with two SVX4 chips at the other end. The hybrid was mounted on the hybrid support structure. A photograph of a detail of the silicon module on the support structure is shown in Fig. 8. Although the hybrid can accommodate two readout chips, only the first readout chip was wirebonded. The first 64 channels of the readout chip were only connected to the analogue cable and the second 64 channels were also connected to the sensor. Of this second set of 64 channels, the last 30 channels were inactive. The DC resistance of the 47 cm long sensor support structure was 12 Ω and the resistance of the ground trace on the analogue cable was 20 Ω. The whole assembly was mounted inside an aluminum Faraday cage. The Faraday cage was placed on copper-clad G10 which was connected to the ground of the readout system and of the HV power supply. The electrical connection between the copper-clad G10 and the Faraday cage was quite good; the DC resistance was measured to be less than 1 Ω.

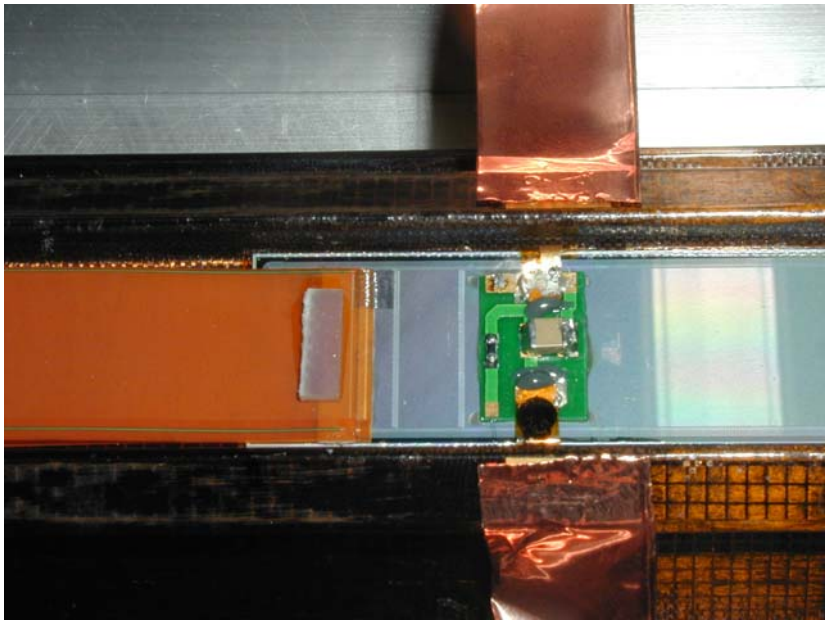

Fig. 8. Photograph showing details of the silicon module mounted on the support structure. Mounted on the sensor is the high voltage filter card with the ground connection. Clearly visible are the ground mesh and the copper connections to the Faraday cage.

6 Test Results

First, the test results of the LØ module before installing it on the prototype support structure are given. This result serves as a reference for the effect of adding the support structure. Next, we present the test results for several different grounding configurations after installation.

We define the noise on the output of a given channel as the standard deviation σ of the digital output in ADC counts for that channel:

$$\sigma_a^2 \; = \; \overline{a^2} - \overline{a}^2 \; . \tag{1}$$

In practice, the quantity σ_a is estimated by computing the root mean square value of the digital output of the channel under consideration over a large number of events (typically 1000). Because we are interested in the susceptibility of the system to external noise sources, we also define the "differential" noise of a given channel as $1/\sqrt{2}$ of the standard deviation of the difference between the output signal a for that channel and the digital output signal a' of a neighboring channel:

$$(\sigma_a^{diff})^2 \; = \; \frac{\overline{(a-a')^2} \; - \; \overline{(a-a')}^2}{2} \tag{2}$$

Again, in practice the quantity σ_a^{diff} is estimated by computing the root mean square value of $(a - a')/\sqrt{2}$ over a large number of events. Assuming that $\sigma_a = \sigma_{a'}$, i.e. that the channel under consideration and its neighbor have the same noise, we have

$$(\sigma_a^{diff})^2 = \frac{\sigma_a^2 + \sigma_{a'}^2}{2} - \overline{aa'} + \overline{a}\,\overline{a'} \tag{3}$$

$$= \frac{\sigma_a^2 + \sigma_{a'}^2}{2} - \rho\,\sigma_a\,\sigma_{a'} \tag{4}$$

$$= \sigma_a^2\,(1 - \rho), \tag{5}$$

where ρ is the correlation coefficient between a and a', $\rho = cov(a, a')/(\sigma_a \sigma_{a'})$. The differential noise is thus equal to the total noise if there is no correlation between the output signals of neighboring channels. A positive correlation can be due to a common component of noise induced by external pickup and is the object of study. Due to capacitive coupling between neighboring strips in the silicon sensor a negative correlation could be present as well at the few percent level [17]. This effect has been neglected here. When the total noise of the device is equal to the differential noise and is the same as the value obtained on the test bench in a Faraday cage, the performance of the system is considered to be optimal.

6.1 Before Installation

The silicon module was tested on the bench inside a Faraday cage. The total noise before installation on the carbon fiber support structure was measured to be 2.7 ADC counts for channels connected to both the sensor and the analog cable with a vanishing correlation coefficient. That is, there was no significant difference between total and differential noise. The bandwidth setting of the SVX4 was such that the 10-90% risetime was measured to be 35 ns and 65 ns for 10 pF and 33 pF capacitive load, respectively. The integration time of the preamplifier was 132 ns. The resulting risetime is fast enough not to collect all charge for the capacitive loads used in the measurements. All results are quoted in ADC counts. For the parameter settings used for our tests the gain of the SVX4 chip is approximately 700 electrons per ADC count. The measured noise of 2.7 ADC counts, or 1890 e^-, is in reasonable agreement with the expected noise, given a strip load capacitance of 1.4 pF/cm.

The total noise before installation on the carbon fiber support structure was 2.7 ADC counts for channels connected to both the sensor and the analog cable. The module was then installed on the support structure without a ground connection and the whole assembly was placed in a Faraday cage. The noise level after installation went up to more than 50 ADC counts, indicating the need for additional grounding.

The ground connection at the hybrid end was then improved by increasing the area of the copper connection between the hybrid and the support structure. The actual ground connection itself, however, was still only established by one wire soldered from the hybrid ground pad to the copper strip. The noise level was reduced to about 14 ADC counts, still considerably higher than the performance on the bench. This indicates a persisting high impedance ground connection. Both resistance and inductance contribute to the impedance, but for high frequencies the inductance often dominates. For the LØ system a high impedance connection is equivalent to a high inductance connection. The inductance was then minimized by soldering additional wires from the hybrid to the support ground. Adding additional wires can be viewed as adding additional inductances in parallel and thus reducing the overall inductance. The impact of this simple solution on reducing the impedance in the ground connection is shown in Fig. 9, which shows the total noise as a function of the number of wires used in grounding the hybrid to the support ground. The wire length is about 4 cm each. Because the resistance of each wire is quite small, much less than the other connections in the ground path, the dependence of the noise on the configuration of the wires is due to the inductance of the wires. Shortening the wire length from 4 cm to approximately 1.5 cm suppresses the noise by about 10%.

The setup was then carefully improved by enlarging the ground connection to the support structure and minimizing its inductance. A noise level equivalent to the bench performance was obtained and sets the reference point for the subsequent noise studies. This grounding configuration is referred to as grounding scheme *i)* below.

The following three grounding schemes were then studied and compared:

i) Grounding of Hybrid: the ground on the hybrid is connected to the hybrid support structure using short, low inductance, copper braid. The support structure itself was connected to the Faraday cage with copper tape. One end of a copper strip was taped to the chassis of the Faraday cage, and the other end to the gold pads on the kapton flex embedded in the support structure. In addition, one end of a thin strip is soldered directly to the

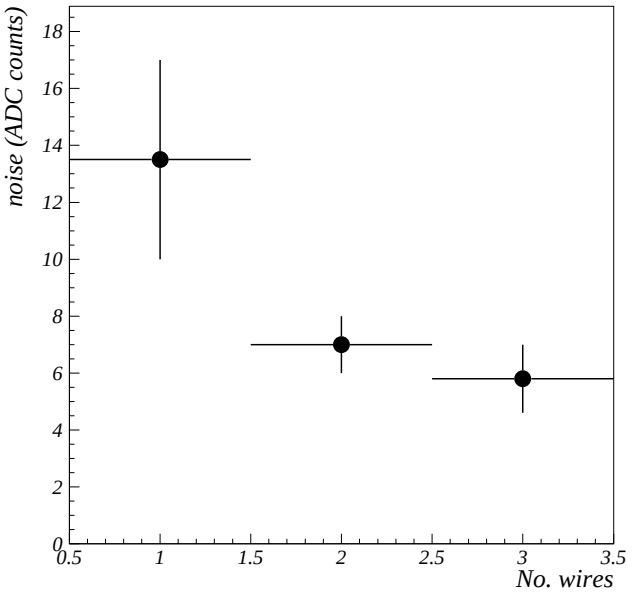

Fig. 9. Noise in terms of ADC counts as a function of number of wires connecting the hybrid ground and the Faraday cage.

ground on the hybrid and the other end taped to the Faraday cage using copper tape.

ii) Grounding of Sensor: the ground on the high voltage filter card is connected to the sensor support structure, which in turn was connected to the Faraday cage with copper tape. One end of a copper strip was taped to the chassis of the Faraday cage, and the other end to the gold pads on the kapton flex embedded in the support structure.

iii) Grounding of both Hybrid and Sensor: combining scheme *i)* and *ii)*.

The noise distributions for the three configurations are shown in Fig. 10. Both the total noise (solid circles) and differential noise (open squares) are plotted. The three configurations have a total noise level of $\sim$2.7, $\sim$120, and $\sim$7 ADC counts, respectively. Recall that the first 64 channels of the readout chip are connected to the analog cable only and that only the second half is connected to both the analog cable and the sensor and that the last 30 channels of this set were inactive.

As described in the beginning of this section, in configuration *i)* utmost attention was paid in establishing good ground connections. The noise performance obtained is identical to the behavior of the module on the bench (see Fig. 10 (top)). An increase in noise is observed at channel 64. Recall that the first 64 channels were only connected to the analogue cable, whereas the following 34 channels were also connected to the sensor. The increase in noise from about 1.8 to 2.7 ADC counts is consistent with the added capacitive load of 11.2 pF

of the silicon strip.

This grounding scheme provides a single-point ground. Theoretically, a single-point ground provides the best grounding configuration. In practice, however, it is difficult to achieve a single-point ground especially for systems like the close-packed LØ structure, because of the tight space constraints. For example, the support structures of nearby detector elements can easily couple to LØ capacitively, resulting in a breakdown of the single-point grounding scheme. Because of the inherent uncertainties when installing a detector as part of a complete system and operating all elements of the system concurrently, it is most prudent to implement a multi-point ground. Therefore grounding schemes *ii)* and *iii)* are pursued and in our application all hybrids and all sensors will be tied to the various ground mesh circuits. The challenge then is to achieve the same noise performance with a multi-point ground.

When grounding occurs only at the sensor end, configuration *ii)*, the noise is at least an order of magnitude worse. As we will explain below, this configuration has the largest ground loop. For configuration *iii)* the differential noise is brought down to the level of about 3 ADC counts, but the coherent noise contribution has about the same magnitude. Also note that the total noise exhibits an odd-even structure, as seen clearly in the bottom graph of Fig 10. The total noise contribution fluctuates from high to low for alternate channels. Recall that the analogue cable is a two layer cable and the channels on each sublayer are all either even or odd. The channels with high common mode noise correspond to the traces on the bottom layer of the analogue cable assembly.

Fig. 11 shows the schematic of an equivalent circuit diagram for the three configurations. The hybrid ground and the sensor ground connections are indicated. Because the ground trace on the analog cable has a substantial resistance of about 20 Ω, the actual signal return is the chassis of the Faraday cage for configurations *ii)* and *iii)* (see Fig. 12). When the hybrid ground connection is broken, corresponding to configuration *ii)*, the signal ground has a very large ground loop through the chassis of the Faraday cage to the hybrid. The setup is very susceptible to any source of noise, as is evident from the center graph in Fig 10. Although in configuration *iii)* the loop is substantially reduced, noise pickup is not eliminated. As is self-evident from Fig. 12, configuration *i)* has the smallest ground loop. Since great care was given in establishing the ground connection for the hybrid end, the effects of the small ground loop were minimized.

High impedance ground connections cause a potential difference between the reference point of the hybrid, or actually the pre-amp in the SVX4 readout chip, and the sensor, resulting in the large noise observed. A low impedance ground connection, in our case equivalent to a low inductance connection, is thus crucial for optimum electrical performance. We also argued that for

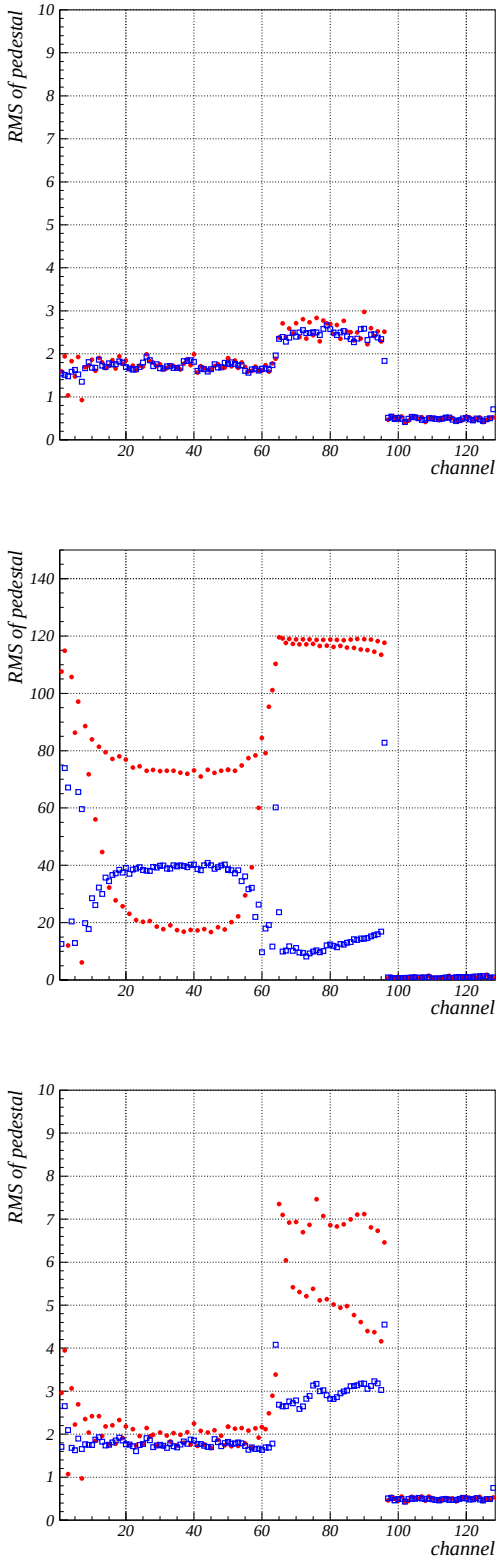

Fig. 10. Noise distribution in ADC counts versus channel number after installing the silicon module onto the support structure. The top, middle, and bottom figures show the distributions corresponding to grounding scheme *i)*, *ii)*, and *iii)*, respectively. The total noise is represented by solid circles, the differential noise by open squares.

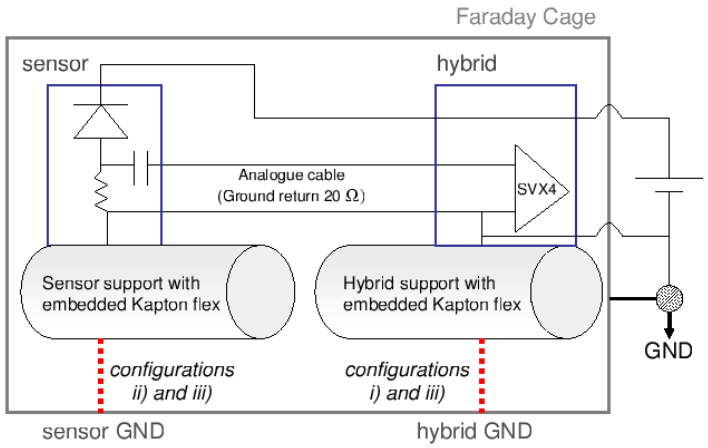

Fig. 11. Schematic equivalent circuit diagram for the test setups.

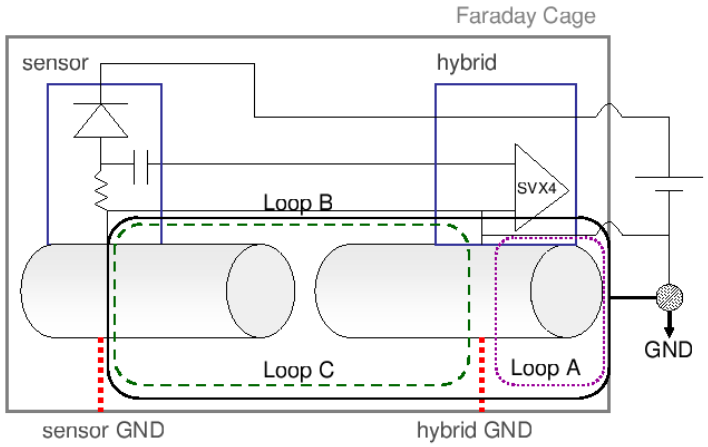

Fig. 12. Indication of ground loops A (dotted), B (solid) and C (dashed) in the equivalent circuit diagram corresponding to grounding configuration *i)*, *ii)* and *iii)*, respectively.

close-packed structures like the LØ structure a multi-point ground is the most conservative approach.

In the next test we established an electrical connection between the sensor and hybrid support structures. One end of a copper ground mesh circuit was

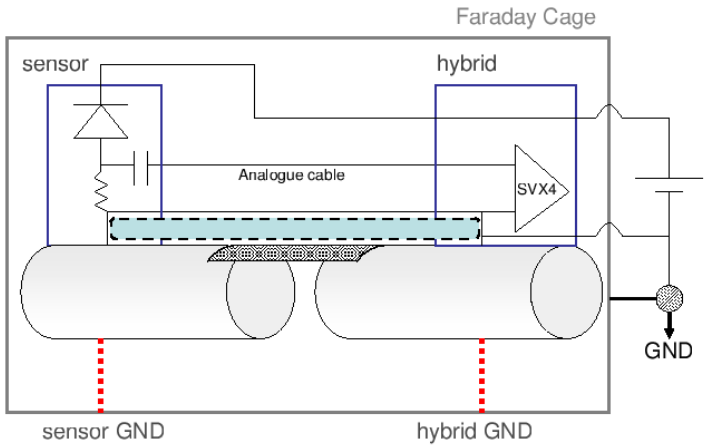

Fig. 13. Equivalent circuit diagram for the final test configuration with additional ground connections between the two support structure.

attached with silver epoxy to the gold pad on the kapton flex circuit that was co-cured onto the sensor support structure and the other end to the gold pad on the hybrid support structure (see Fig. 7). This minimizes the area of the ground loop. The ground return is now a continuous, low inductance mesh circuit in close proximity to the analogue cable and the hybrid. The equivalent circuit diagram is shown in Fig. 13. The resulting noise distribution is identical to the one shown in the top graph in Fig. 10. The average rms of the pedestal is again 2.7 ADC counts. This proves that the grounding scheme we developed is adequate. Note that, due to the double stack configuration of the analogue cable, a small odd-even effect in the pedestal distribution persists: the readout channels in the bottom layer of the analogue cable are more susceptible to external noise and have a larger pedestal rms value. The assumption which lies at the basis of equation 5, namely that the rms of neighboring channels is the same, is not completely valid in this situation. Odd and even channels have different proximity to the ground plane and thus an intrinsic different noise behavior.

7 General Grounding Scheme

The general principle of grounding a detector states that a single-point grounding scheme gives better noise performance than a multi-point one. Because of tight space constraints, however, it is often difficult to achieve a single-point ground. For example, any kind of support structure close to the detector can

easily couple to the active elements capacitively, resulting in the breakdown of the single-point grounding scheme. It is therefore good engineering practice to implement a multi-point ground.

We have developed a method of integrating grounding circuits in a carbon fiber support structure. We have demonstrated that embedding copper-kapton mesh circuits in the various support elements, with the copper covering more than 15% of the area, is a flexible way of providing ground connections and is extremely robust. Our test results indicate that there are two key requirements for low noise performance: the ground loop must be minimized, and there must be a low impedance ground connection between the active detector and the front-end readout electronics.

For the LØ silicon detector at small radius being proposed for the DØ experiment, these general grounding principles have been implemented and excellent results were obtained. A copper-kapton mesh circuit was embedded in the sensor support structure with the kapton covering the total surface area and the coper having an area coverage of 30%. With this ground mesh embedded in the surface of the support structure it was straightforward to make low inductance ground connections to the sensor using small copper-kapton jumper cables attached to precisely positioned gold plated pads in the ground mesh using silver epoxy.

To minimize the inductance of the ground path, a uniform continuous ground plane between the sensor and hybrid is needed. Another copper-kapton mesh circuit, with the same specifications, was embedded in the hybrid support structure. Small copper-kapton jumper cables attached to gold-plated pads at the end of either support structure provided the electrical connection between them. All hybrids and all sensors are thus tied to one uniform ground mesh. Grounding the hybrid was a bit more difficult due to space constraints. Based on the rule of low inductance connections, the shortest path from the hybrid to the inner support cylinder is needed. This has led to a design where the hybrid has a ground strip at the bottom which makes direct contact with the support structure.

8 Carbon Fiber Conductivity

In this paper a pragmatic approach has been taken in the design of electrically robust detectors using carbon fiber. It is still an intriguing question why carbon fiber is so highly conductive at high frequencies. We speculate that this is due to the large skin depth. Carbon fiber consists of strands of conductor embedded in a non-conductive epoxy. This configuration nearly eliminates eddy currents, which otherwise would reduce conductivity limiting it to the surface. It is

similar to the use of plates in conventional motors or transformers to get rid of eddy currents. Without eddy currents, the area available for conduction in carbon fiber is much thicker than for a similar amount of copper. This conjecture, however, needs to be experimentally verified.

9 Conclusion

A low inductance grounding scheme with the smallest possible ground loop is essential to achieve low noise performance. This implies the use of short and wide electrical connections, and a careful mechanical design to minimize or eliminate ground loops. We have shown that for frequencies relevant for operation of silicon detectors in the Tevatron environment, carbon fiber is a good conductor and cannot be distinguished from copper. We have demonstrated that the use of copper-kapton flexible mesh circuits, with the copper covering more than 15% of the surface, provides adequate electrical coupling to carbon fiber support elements. Co-curing these circuits with the carbon fiber during the lay-up process provides an electrically integrated support, with great flexibility to adopt to the specific electrical requirements for that application. In a future paper the results of extensive tests on a small radius silicon detector, following the design rules outlined above, will be presented.

10 Acknowledgments

We wish to thank Colin Daly, Bill Kuykendall, Henry Lubatti, Joshua Wang and Tianchi Zhao from the University of Washington for the manufacturing of the carbon fiber structures, Jim Fast, Kurt Krempetz, Mike Hrycyk and Frank Lehner for valuable advice, Bert Gonzalez for the assembly of the modules and all our DØ silicon colleagues for helpful discussions.

References

[1] P. Chochula et al., DELPHI Silicon Tracker Group, Nucl. Instrum. Meth. A **412**, 304 (1998)

[2] C. Bozzi et al., BABAR Collaboration, Nucl. Instrum. Meth. A **453**, 78 (2000)

[3] A. Affolder et al., CDF Collaboration, Nucl. Instrum. Meth. A **461**, 216 (2001)

[4] CERN/LHCC 98-6, CMS Collaboration, CMS Tracker Technical Design Report, April 1998
CERN/LHCC 2000-016, February 2000.

[5] T. Nelson, CDF Collaboration, Int. J. Mod. Phys. **A16S1C**, 1091 (2001)

[6] C. Hill, CDF Collaboration, Nucl. Instrum. Meth. A **511**, 118 (2003).

[7] DØ Run IIb Silicon Detector Technical Design Report, Fermilab, Pub-02-327-E.

[8] Research Institute of Materials Science and Technology (RIMST-ELMA), Moscow, Zelenograd, 103460.

[9] Dyconex AG, Grindelstraße 40, CH-8303 Bassersdorf, Switzerland

[10] ANSYS engineering simulation software, ANSYS Inc., Southpointe 275 Technology Drive, Canonsburg, PA 15317

[11] M. Garcia-Sciveres *et al.*, Nucl. Instrum. Meth. A **511**, 171 (2003).

[12] AVX Corporation, Kyocera Group, PO Box 867, Myrtle Beach, South Carolina 29578.

[13] Bryte Technologies, Inc. 18410 Butterfield Blvd., Morgan Hill, CA 90537.

[14] YLA, Inc., 2970 Bay Vista Court Benicia, CA 94510.

[15] P.J. Walsh, in: D.B. Miracle and S.L. Donaldson (Eds.), ASM Handbook, Vol. 21: Composites, ASM International, Amsterdam, 2001, Sec. 2.

[16] Compunetics Inc., 700 Seco Road, Monroeville, PA 15146.

[17] G. Lutz, Nucl. Instrum. Meth. A **309**, 545 (1991)